

## Electronic Supplementary Information

### ***Operando* electrochemical study of charge carrier processes in water splitting photoanodes protected by atomic layer deposited TiO<sub>2</sub>**

Wei Cui,<sup>1</sup> Thomas Moehl<sup>1</sup>, Sebastian Sio<sup>2</sup> and S. David Tilley<sup>\*1</sup>

1. Department of Chemistry, University of Zurich, Winterthurerstrasse 190, CH-8057 Zurich, Switzerland
2. Empa – Swiss Federal Laboratories for Materials Science and Technology, Uerlandstrasse 129, CH-8600 Dübendorf, Switzerland

\*E-mail: david.tilley@chem.uzh.ch.

## **Experimental**

### **Si wafer cleaning**

(111)-oriented np<sup>+</sup>Si and pn<sup>+</sup> wafers (thickness ~0.5 mm) were purchased from PrimeWafers. For np<sup>+</sup>Si wafers, the n-Si substrate was lightly phosphorous-doped ( $10^{16}$  cm<sup>-3</sup>) and a 2 μm-thick heavily p<sup>+</sup>-type surface layer (polished) was doped with boron ( $10^{19}$  cm<sup>-3</sup>). For pn<sup>+</sup>Si wafers, the n-Si substrate was lightly boron-doped ( $10^{16}$  cm<sup>-3</sup>) and a n<sup>+</sup>-type surface layer (polished) was phosphorus doped ( $10^{19}$  cm<sup>-3</sup>). Double-polished n-Si wafers (Sil'tronix) were phosphorous-doped with a dopant density of  $10^{16}$  cm<sup>-3</sup>. The wafers were cut into  $2.5 \times 1$  cm<sup>2</sup> pieces followed by sequential sonication in acetone, ethanol and MilliQ water (18 MΩ) for 10 minutes each. Then a two-step deep cleaning was accomplished by using a 5:1:1 mixture of H<sub>2</sub>O:NH<sub>4</sub>OH:H<sub>2</sub>O<sub>2</sub> and a 5:1:1 mixture of H<sub>2</sub>O:HCl:H<sub>2</sub>O<sub>2</sub>, both in 50 °C water bath for 10 minutes, in order to completely remove organic and inorganic contaminants. To etched away the native oxide layer, wafers were finally dipped in 2% HF for 30 s, followed by rinsed with deionized water and dried under N<sub>2</sub> stream for the ALD-TiO<sub>2</sub> deposition.

### **Atomic layer deposition of TiO<sub>2</sub>**

100 nm thick TiO<sub>2</sub> on the Si wafer was deposited by atomic layer deposition (ALD) using a Picosun R200 tool. The as-cleaned wafers were placed inside the ALD chamber, which was already heated to 120 °C. Tetrakis(dimethylamino)titanium (TDMAT, Sigma-Aldrich) and H<sub>2</sub>O were used as the precursor for Ti and O, respectively. TDMAT was heated to 85 °C and a 1.6 s pulse was used (with software boost function), followed by a 6.0 s N<sub>2</sub> purge. H<sub>2</sub>O was held at room temperature and a 0.1 s pulse was used, followed by a 6.0 s N<sub>2</sub> purge. The growth rate of TiO<sub>2</sub> is around 0.54 Å per TDMAT-H<sub>2</sub>O cycle. To deposit 50, 70, 100

and 170 nm TiO<sub>2</sub>, 930, 130, 1860 and 3160 TDMAT-H<sub>2</sub>O cycles were carried out, respectively. Measurement of the thickness of ALD-TiO<sub>2</sub> deposited on a piece of Si witness wafer was carried out by ellipsometry (alpha-SE, J.A. Woolam Co.), and fitted with a model for transparent films on Si wafers.

### **Fabrication of DWEs**

Generally, the back contact (the first working electrode or WE1) was made to the back side of the silicon by scratching the wafer, smearing Ga–In eutectic (Aldrich) and attaching a conductive copper wire. A layer of epoxy resin (Loctite Epoxide-resin EA 9461) was then used to cover and glue the wafer to a glass microscope slide, with a certain portion of the front surface left uncovered as the electrochemical active area. For making the front contact, a 20 nm-thick Au layer was sputtered (Safematic CCU-010) onto the epoxy as well as a small part of the exposed TiO<sub>2</sub>. A copper wire was connected to the Au layer with Ag paint (Ted Pella, Inc.) on top of the epoxy, serving as the second working electrode (WE2). Finally, WE2 was protected from the electrolyte solution by masking it with another epoxy layer. In V<sub>2</sub>-controlled PEIS measurements, WE2 was connected to the p<sup>+</sup>Si layer instead of TiO<sub>2</sub>, as drawn in Fig. S4

The pn<sup>+</sup>Si/TiO<sub>2</sub> DWE were fabricated via the same methods except that WE2 connects to the p<sup>+</sup>Si surface. In terms of nSi/TiO<sub>2</sub> DWE, WE2 is the sputtered 20 nm Au layer attached onto the TiO<sub>2</sub> surface, as drawn in Fig. S9

## Electrocatalyst deposition

For nSi/TiO<sub>2</sub> and np<sup>+</sup>Si/TiO<sub>2</sub> photoanodes, Ni metal layers (2 nm) was deposited onto the surface by sputtering. A working current of 30 mA and a working pressure of 8E-3 mbar were applied.

For pn<sup>+</sup>Si/TiO<sub>2</sub> photocathode, 2 nm-thick Pt catalyst was deposited by sputter as well with a working current of 30 mA and a working pressure of 5E-2 mbar.

## Photoelectrochemical Measurements

Photoelectrochemical measurements were performed in a four-electrode configuration using a BioLogic SP-300 bipotentiostat. The reference electrode was Ag/AgCl (0.197 V vs. NHE) and a Pt wire served as the counter electrode. 1 M KOH and 0.5 M H<sub>2</sub>SO<sub>4</sub> were used for photoanode and -cathode measurements, respectively. All electrode potentials were converted into RHE scale: at room temperature,  $V_{\text{RHE}} = V_{\text{NHE}} + 0.059 \times \text{pH} = V_{\text{Ag/AgCl}} + 0.059 \times \text{pH} + 0.197$ . Simulated one sun illumination (100 mW cm<sup>-2</sup>) was provided by a 150 W Xe-lamp with AM 1.5 G filter from LOT Oriel and a 414 nm cutoff filter was use to avoid the excitation of TiO<sub>2</sub> layer.<sup>a</sup> The light intensity was calibrated with a standardized silicon diode from PV Measurements (USA).

J-V1 and J-V2 curves were obtained from cyclic voltammograms (CVs) collected by sweeping the back contact potential (V1) or the surface potential (V2), respectively, with

---

<sup>a</sup> We note that all measurements were essentially the same with or without the UV filter. Although one might expect that an excitation of the TiO<sub>2</sub> by the UV part of the solar spectrum may result in a decoupling of the Fermi level of the TiO<sub>2</sub> from the p<sup>+</sup>Si underneath (*i.e.* a flattening of the band bending in the TiO<sub>2</sub>), this effect would not be dramatic considering the small fluxes of the UV photons involved relative to the water splitting photocurrents observed, and thus we propose that the mechanism of charge transfer through the conduction band of TiO<sub>2</sub> would remain the same.

the other kept at open circuit. V1 stepwise measurements were performed by potential step chronoamperometry (CA). Each V1 potential step had a duration of 30 s. V2 was synchronously kept at open circuit to record the potential values against the reference electrode.

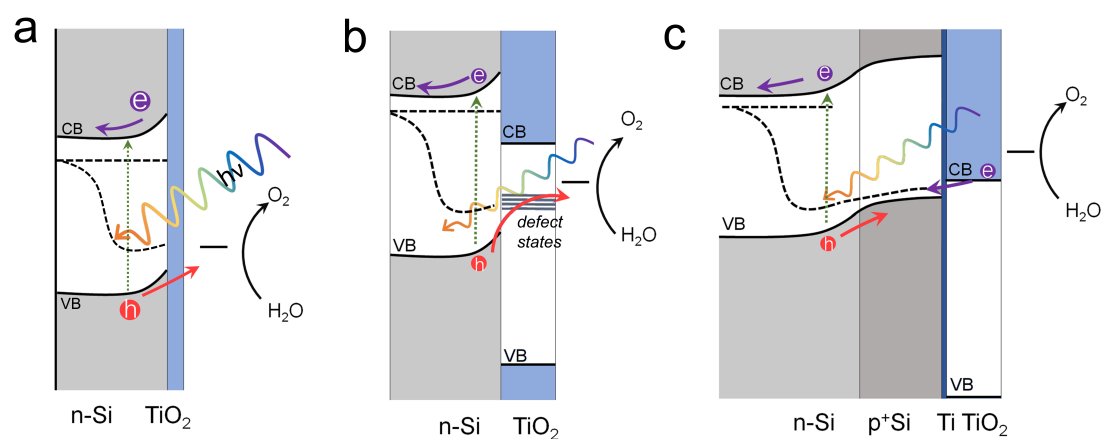
### **PEIS measurements**

Photoelectrochemical impedance measurements (PEIS) were performed during the voltage scanning in the desired potential window in steps of 50 mV with a 60 s equilibrium time at each bias potential step. The frequency range was from  $10^{-1}$  Hz to  $10^6$  Hz and an oscillating voltage of 15 mV was applied. For photoanode, PEIS were recorded in 1.0 M KOH and 0.5 M H<sub>2</sub>SO<sub>4</sub> for photocathode. PEIS data were further fitted with ZView software (Scribner). For all spectra fitting process, a constant phase element (CPE) accounts for capacitance. Note that all impedance study we show in this work are only based on the resistance rather than capacitance. Because the semicircle features of Nyquist plots can be fitted with different CPE contribution, where the capacitive contribution can be various but resistive contribution is similar. This makes the resistance-based study more reliable.

The flat band potential ( $E_{FB}$ ) of the ALD-TiO<sub>2</sub> layer was determined with a Mott Schottky plot, which was derived from an EIS measurement in a three-electrode configuration under dark condition. The working electrode was a fluorine-doped tin oxide (FTO)-coated glass with a 100 nm-thick ALD TiO<sub>2</sub> layer. The counter and reference electrodes were a Pt wire and a Ag/AgCl electrode, respectively. The Electrolyte solution used was 1 M H<sub>2</sub>SO<sub>4</sub>. The space charge capacitances ( $C_{sc}$ ) were extracted from the fitting

of Nyquist plots under applied potentials, thus no frequency dispersion appears in the Mott Schottky plot.

The built-in voltage ( $V_{bi}$ ) of the nSi/TiO<sub>2</sub> junction was conducted with a similar Mott-Schottky method as described above but using a two-electrode mode under dark condition (without electrolyte solution). One of the electrodes was connected to the back contact of the nSi/TiO<sub>2</sub> electrode. The other one was connected to the front contact, which was a 20 nm-thick Ni metal layer sputtered onto the TiO<sub>2</sub> surface.



**Scheme S1** Three possible mechanism for the “hole-leaky” property of TiO<sub>2</sub>. (a) A thin tunnelling TiO<sub>2</sub> layer; (b) holes transfer through defect states; (c) electron transfer through the conduction band.

### Determination of band structures of nSi, p<sup>+</sup>Si and ALD-TiO<sub>2</sub>.

The Fermi level of nSi and p<sup>+</sup>Si are determined by equation (1) and (2), respectively.

$$E_{CB} - E_{FB} = \frac{kT}{q} \ln\left(\frac{N_D}{N_C}\right) \quad (1)$$

$$E_{FB} - E_{VB} = \frac{kT}{q} \ln\left(\frac{N_V}{N_A}\right) \quad (2)$$

Where  $N_C$  and  $N_V$  are the effective density of states in the Si conduction band ( $\sim 2.8 \times 10^{19} \text{ cm}^{-3}$ ) and valence band ( $\sim 1.2 \times 10^{19} \text{ cm}^{-3}$ ), respectively.  $q$  is the electron charge,  $k$  is the Boltzmann constant and  $T$  is the temperature in Kelvin. For Si,  $E_{CB}$  and  $E_{VB}$  locate at  $\sim -0.5$  and  $0.6$  eV versus RHE, respectively.<sup>1</sup> The donor density ( $N_D$ ) of nSi is  $10^{16}$  and the acceptor density ( $N_A$ ) of p<sup>+</sup>Si is  $10^{19} \text{ cm}^{-3}$ . Therefore,  $E_{CB} - E_{FB}$  is  $\sim -150$  mV, which means that the nSi fermi level locates 150 mV lower than the conduction band. In terms of p<sup>+</sup>Si,  $E_{FB} - E_{VB}$  is almost 0, suggesting that the high acceptor density makes the Fermi level location extremely close to the valence band edge.

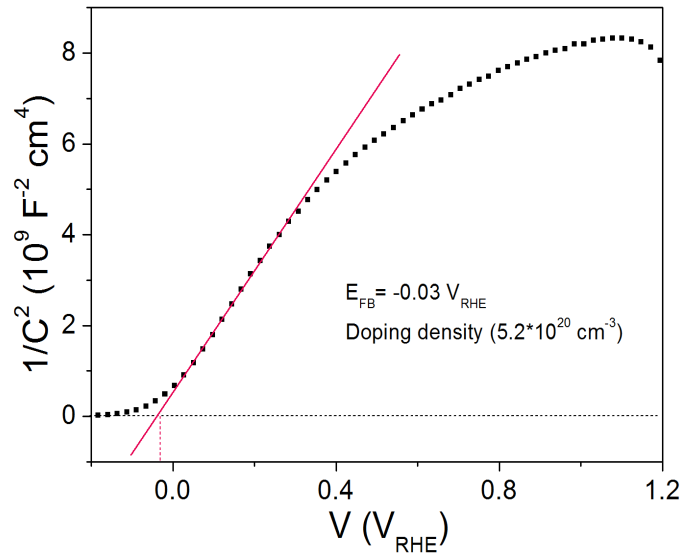


**Fig. S1** The Mott–Schottky plot for ALD-TiO<sub>2</sub> (100 nm on FTO), measured in 1 M H<sub>2</sub>SO<sub>4</sub>

The actual Fermi level position of ALD-TiO<sub>2</sub> was determined by the Mott Schottky plot ( $1/C_{sc}^2$  plotted versus the applied potential). The linear part fitting is related to the equation is shown below:

$$\frac{1}{C_{SC}^2} = \frac{2}{N_D \epsilon \epsilon_0 q} \left( E - E_{FB} - \frac{kT}{q} \right) \quad (3)$$

Where  $E$  is the applied potential,  $\epsilon$  is the dielectric constant (here is 38 for ALD-TiO<sub>2</sub>) and  $\epsilon_0$  is the permittivity of vacuum.<sup>2</sup>  $C_{sc}$  is the space-charge capacitance.  $N_D$  is the doping density of ALD-TiO<sub>2</sub>, which can be obtained from the slope of equation (3). The positive slope suggests the n-type doping and the x-intercept is indicative of the  $E_{FB}$ . By applying equation (3), a  $E_{FB}$  of  $-0.03 \text{ V}_{RHE}$  and a  $N_D$  density of  $5.2 \times 10^{20} \text{ cm}^{-3}$  can be determined. Applying equation (1) results in a CB which locates slightly higher than  $E_{FB}$ .  $N_C$  of ALD-TiO<sub>2</sub> is  $7.8 \times 10^{20}$ .<sup>3</sup> Since  $E_{FB}$  refers to the applied voltage that results in no band bending,  $E_{FB}$  is actually the Fermi level position of the semiconductor. Thus, the Fermi level of ALD-TiO<sub>2</sub> is located at  $-0.03 \text{ V}_{RHE}$ .

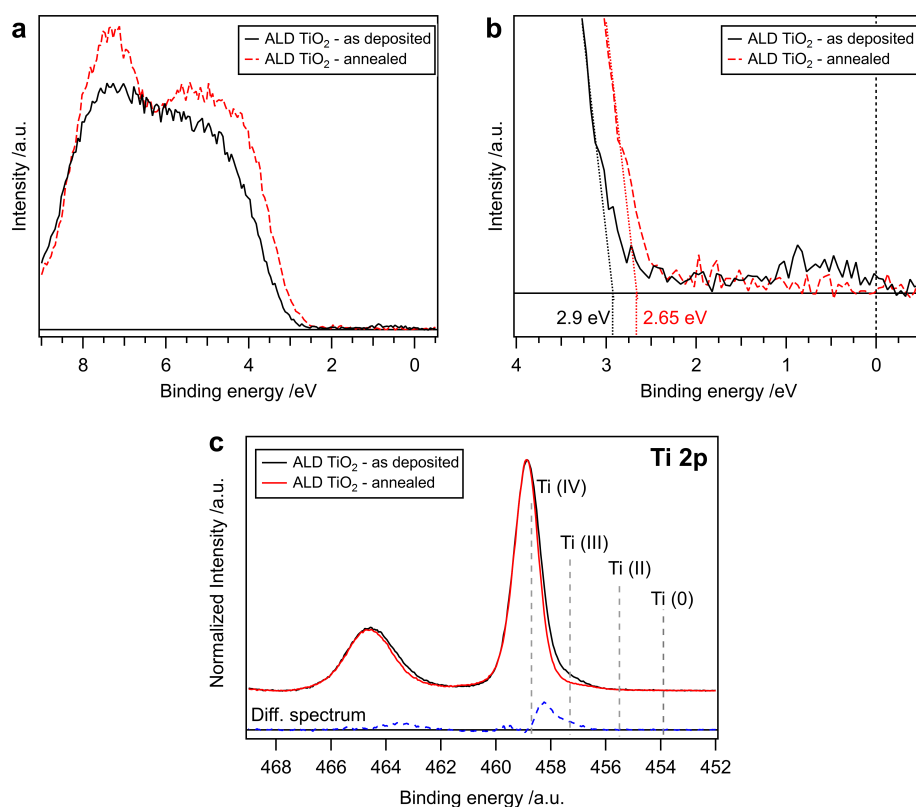


**Fig. S2** X-ray photoelectron spectroscopy (XPS) analysis of ALD-TiO<sub>2</sub>. (a) and (b) valence band spectra. The valence band maximum  $E_{VBM}$  is determined by leading edge extrapolation. Both the as-deposited and annealed samples show n-type doping with  $E_F - E_{VBM} = 2.9$  eV and 2.65 eV, respectively. (c) Normalized Ti 2p core level emission. The annealed sample shows a reduction of the Ti(III) component indicating oxidation of the specimen. No metallic Ti(0) is present in either film. Reference data taken from the NIST database.<sup>4</sup>

XPS on the valence band region reveals n-type doping for both as-deposited and annealed ALD-TiO<sub>2</sub> samples with  $E_F - E_{VBM} = 2.9$  eV and 2.65 eV, respectively. The as-deposited sample shows a defect emission in the mid-gap region around 1 eV (Fig. S2). These types of mid-gap defect states have previously been reported by other groups,<sup>5,6</sup> and are often correlated with the presence of oxygen deficiency in TiO<sub>2</sub>.<sup>7</sup> Core level spectra of the Ti 2p region indicate that the ALD-TiO<sub>2</sub> investigated in this work shows a similar behavior (Fig. S2c). The untreated TiO<sub>2</sub> shows the presence of III-valent Ti, likely due to the presence of oxygen vacancies. After annealing both the defect band and the Ti(III) emission disappear indicating further oxidation of the specimen. In addition, no TiO or metallic Ti are present in either sample.

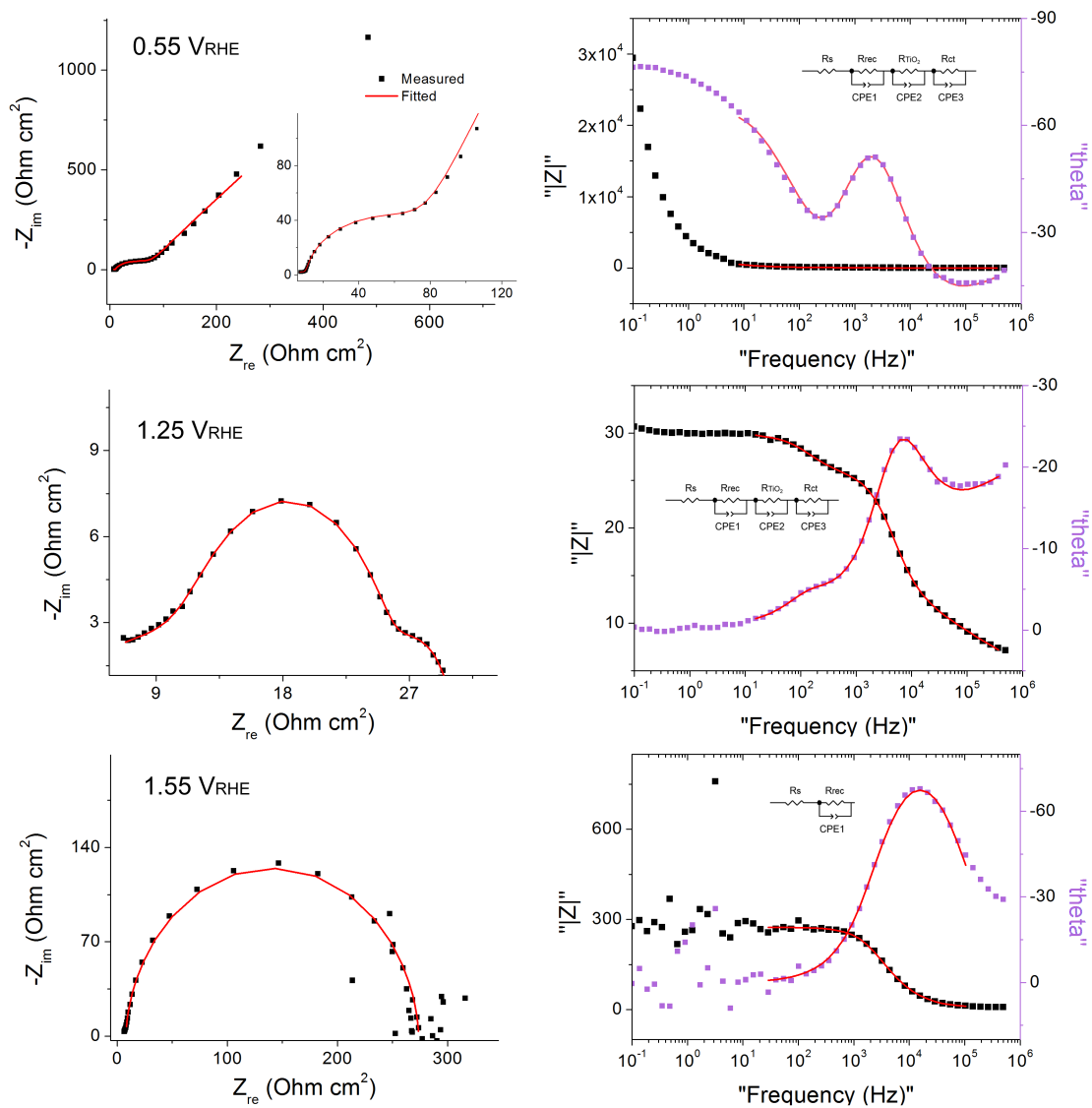


**Fig. S3** Nyquist and bode plots and corresponding fitting of an  $\text{np}^+\text{Si}/\text{TiO}_2/\text{Ni}$  photoanode at back contact potentials of 0.55, 1.25 and 1.55  $V_{\text{RHE}}$  under one sun illumination. Equivalent circuit models are given as well.  $R_s$  is the series resistance raised by electrolyte solution.  $R_{\text{rec}}$  is the overall resistance of charge recombination taking place in the absorbers.  $R_{\text{TiO}_2}$  is the overall resistance of charge transfer through the  $\text{TiO}_2$  layer.  $R_{\text{ct}}$  is associated with the oxygen-evolving process at the Ni catalyst surface.

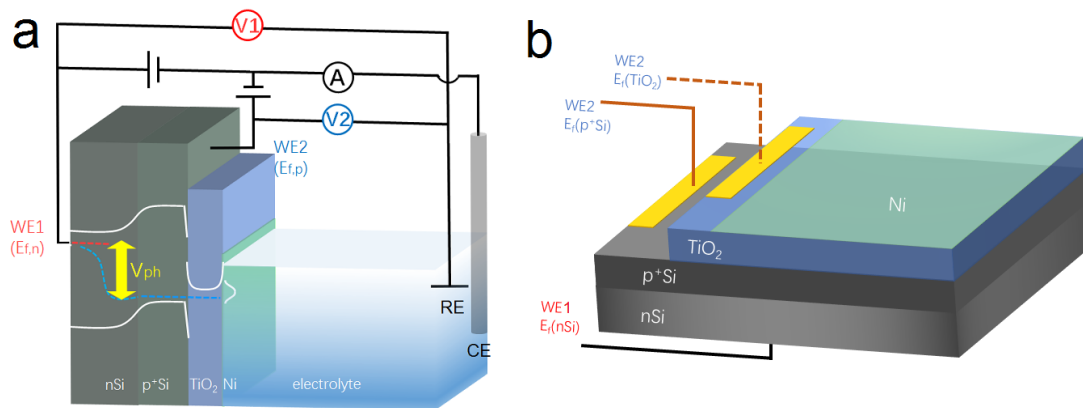


**Fig. S4** (a) Schematic illustration of  $np^+Si/TiO_2/Ni$  DWE. For back contact potential ( $V_1$ ) controlled measurements (CV and EIS), front contact potential ( $V_2$ ) was kept at open circuit. For the  $V_2$  controlled measurements,  $V_1$  was kept at open circuit.  $V_1$  and  $V_2$  also represent the quasi Fermi levels of majority carriers in  $nSi$  (electron) and  $p^+Si$  (hole), respectively.<sup>8</sup> (b) Schematic of the dual working electrode experiment, either connected to the  $p^+Si$  or  $TiO_2$  surface via a 20 nm-thick Au layer. The second working electrode is protected from direct contact to the electrolyte solution by coating with epoxy, which is omitted here for clarity.

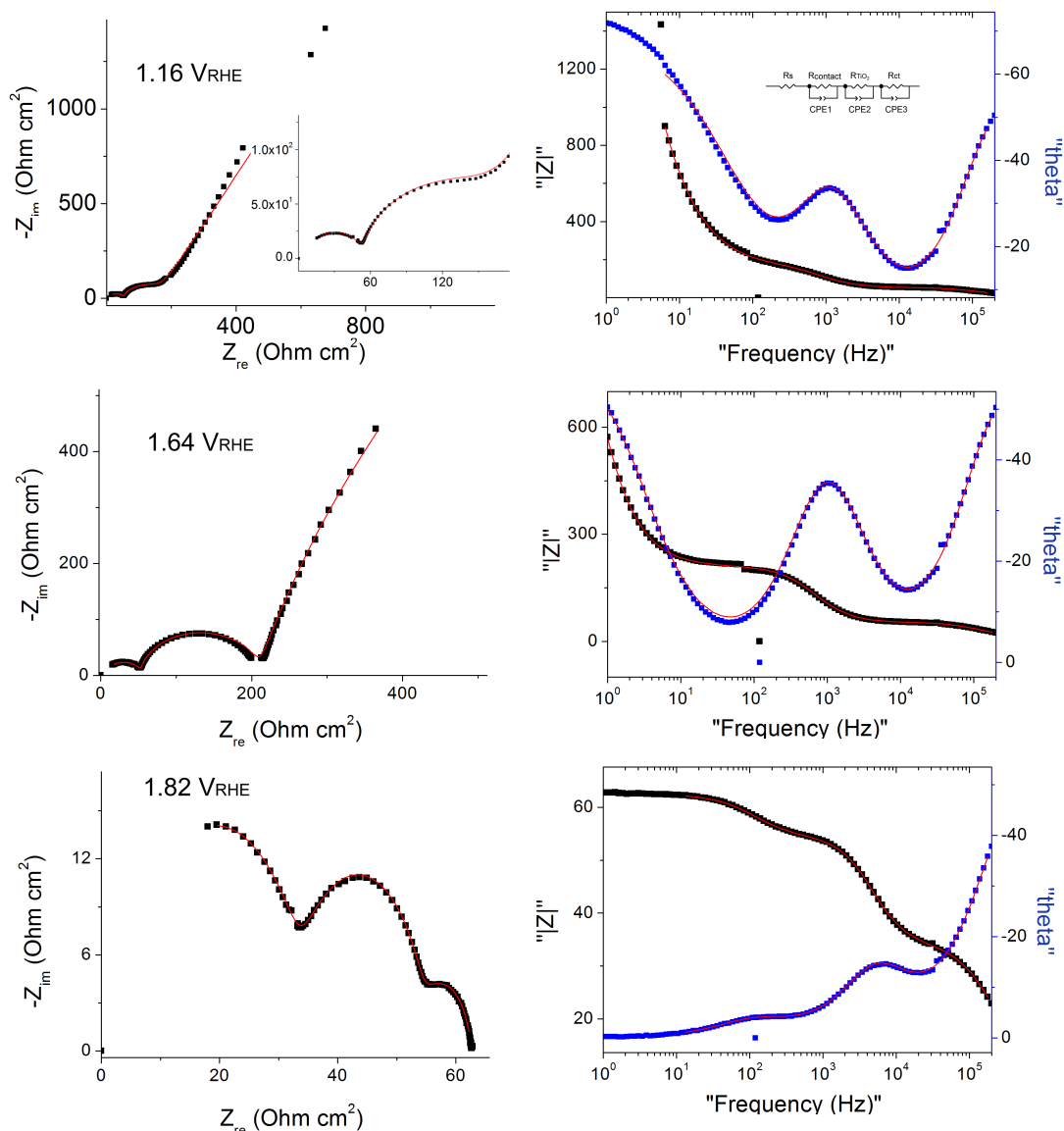


**Fig. S5** Nyquist and bode plots from V2-controlled PEIS measurements and corresponding fitting of an  $\text{np}^+\text{Si}/\text{TiO}_2/\text{Ni}$  photoanode at V1 of 1.16, 1.64 and 1.82  $V_{\text{RHE}}$  under one sun illumination. In V2-controlled PEIS measurements, charges flow from front contact to  $\text{p}^+\text{Si}$  layer, then transfer through the  $\text{TiO}_2$  layer and finally reach the surface to the Ni Catalyst. V2 was kept at open-circuit.

Same equivalent circuit models adopted.  $R_s$  is the series resistance raised by electrolyte solution.  $R_{\text{contact}}$  is the resistance of front contact and charge transfer in  $\text{p}^+\text{Si}$ .  $R_{\text{TiO}_2}$  is the overall resistance of charge transfer through the  $\text{TiO}_2$  layer.  $R_{\text{ct}}$  is associated with the oxygen-evolving process at the Ni catalyst surface.

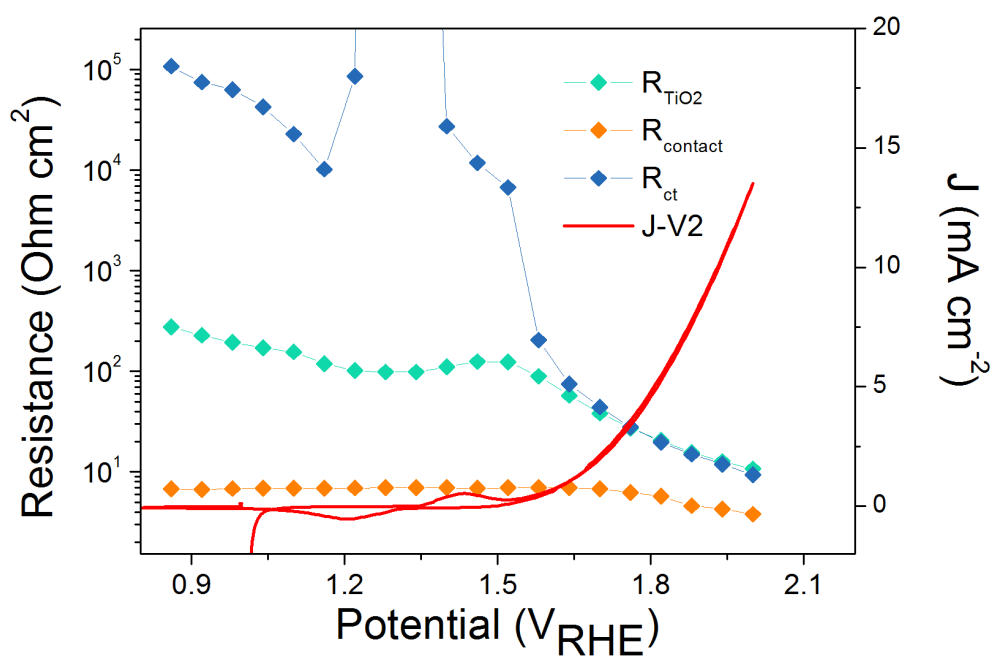


**Fig. S6** Resistances and photocurrent densities ( $J$ ) versus  $V_2$ .  $R_{contact}$ ,  $R_{TiO_2}$  and  $R_{ct}$  were obtained from fittings of Nyquist plots (Fig. S5).  $R_s$  was not plotted here.

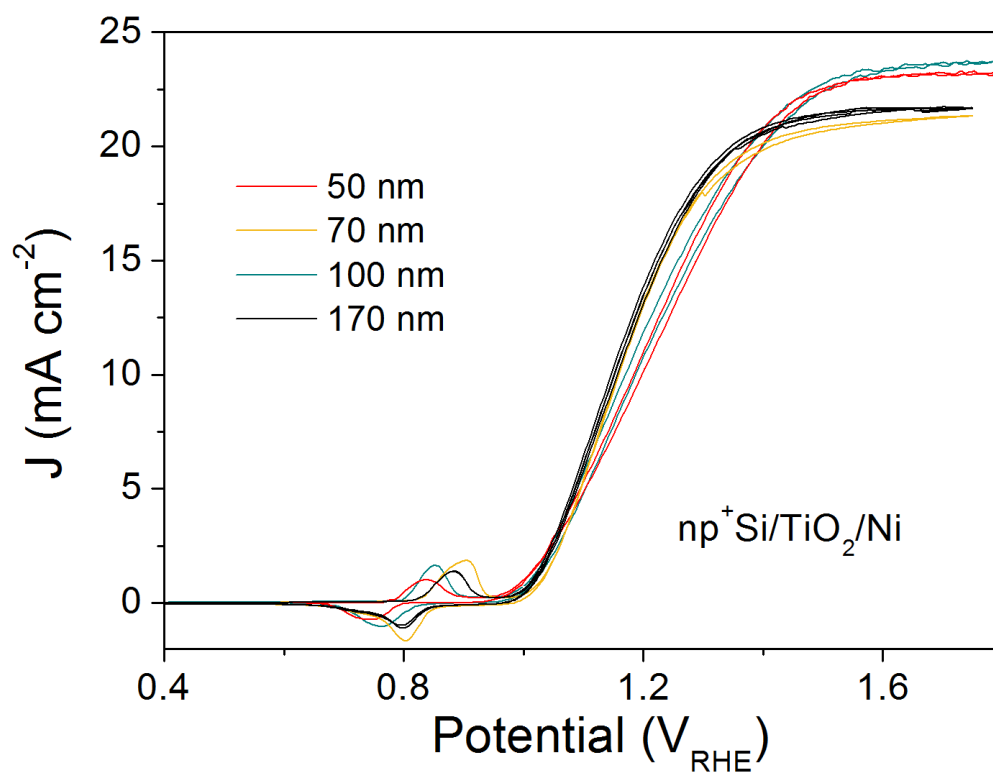


**Fig. S7** CVs of  $np^+Si/TiO_2/Ni$  photoanodes with various  $TiO_2$  thickness.

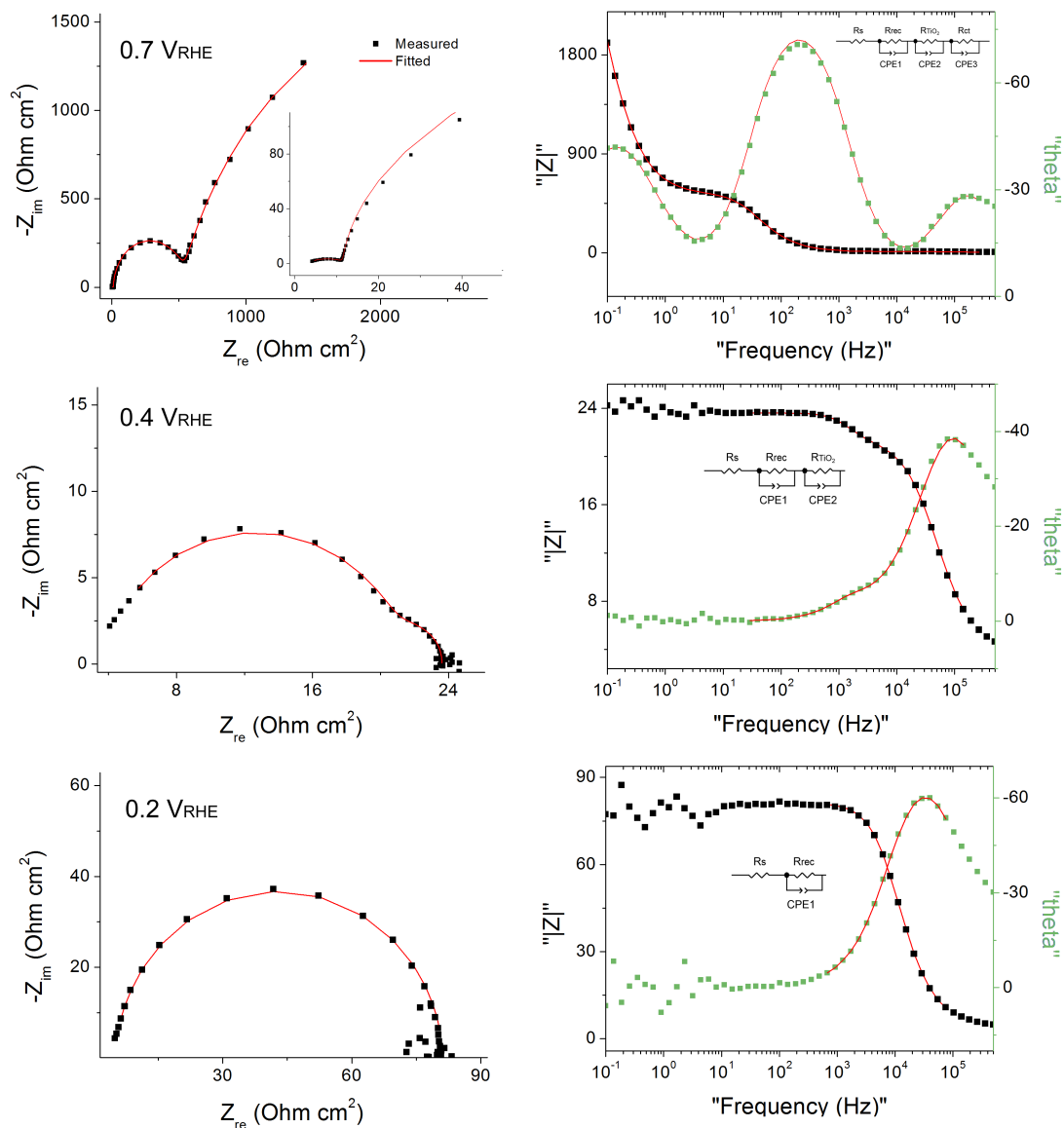


**Fig. S8** Nyquist and bode plots and corresponding fitting of an  $\text{pn}^+\text{Si}/\text{TiO}_2/\text{Pt}$  photocathode at back contact potentials of 0.7, 0.4 and 0.2  $V_{\text{RHE}}$  under one sun illumination. Equivalent circuit models are given as well.  $R_s$  is the series resistance raised by electrolyte solution.  $R_{\text{rec}}$  is the overall resistance of charge recombination taking place in the  $\text{pn}^+\text{Si}$  homojunction.  $R_{\text{TiO}_2}$  is the overall resistance of charge transfer through the  $\text{TiO}_2$  layer.  $R_{\text{ct}}$  is associated with the  $\text{H}_2$ -evolving process at the Pt catalyst surface.

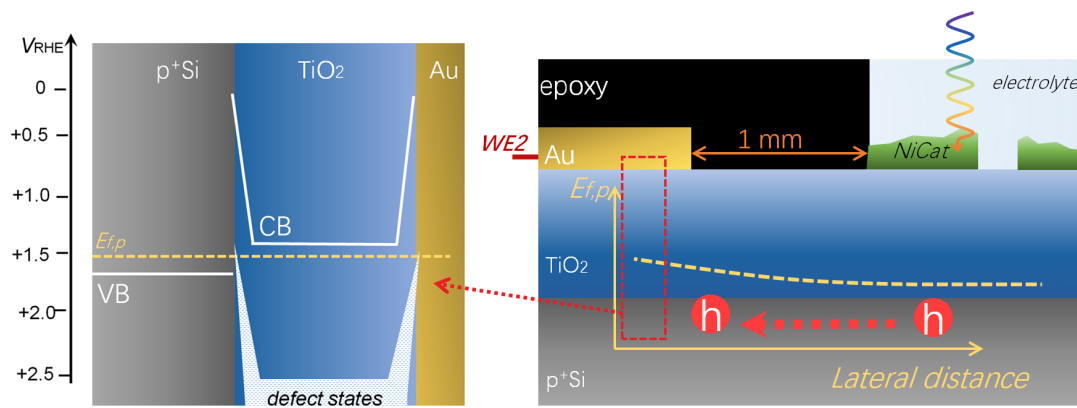


**Fig. S9** Schematic illustration of the quasi Fermi level of holes ( $E_{f,p}$ ), sensed by WE2. The dashed red marking shows the region where band bending at the Si/ $TiO_2$ /Au interfaces is depicted (on the left).

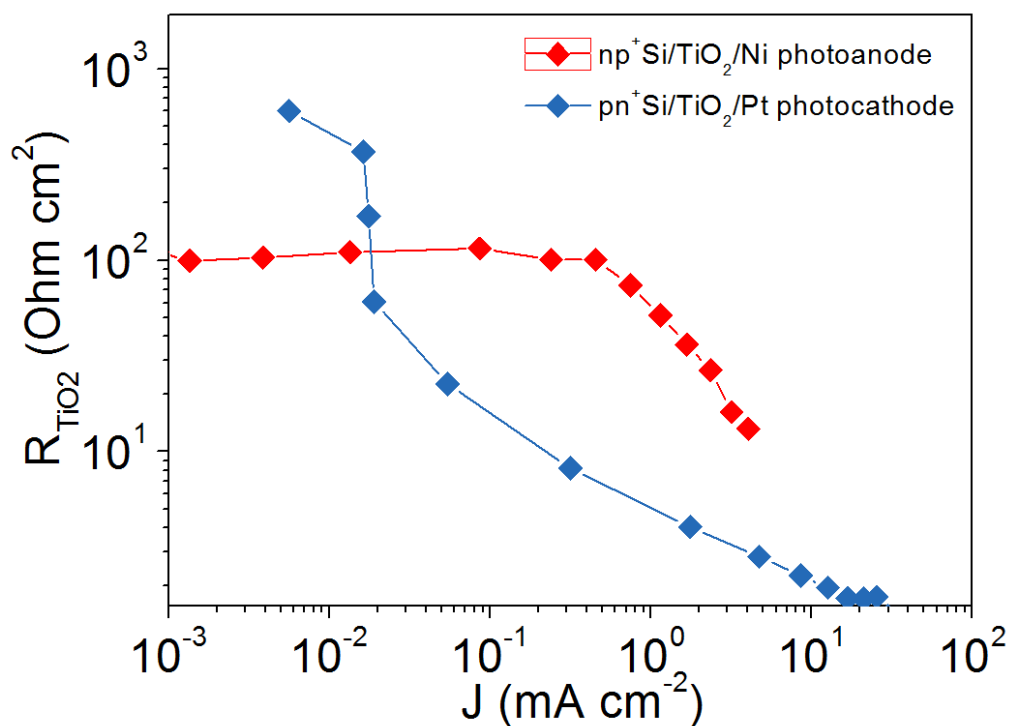


**Fig. S10** Comparison of  $R_{\text{TiO}_2}$  (vs. photocurrent density) values obtained from the  $\text{np}^+\text{Si}/\text{TiO}_2/\text{Ni}$  photoanode and the  $\text{pn}^+\text{Si}/\text{TiO}_2/\text{Pt}$  photocathode. ALD- $\text{TiO}_2$  thickness is 50 nm. The photocurrent density values used in Fig. S9 were the mean value of each potential step during the PEIS measurements.

### Morphology characterization.

The morphology of 100 nm ALD-TiO<sub>2</sub>, NiCat before and after all PEC tests were examined by scanning electron microscopy (SEM, Zeiss Supra 50 VP) and atomic force microscopy (AFM, Asylum Research). All samples were deposited onto the Si wafer substrate.

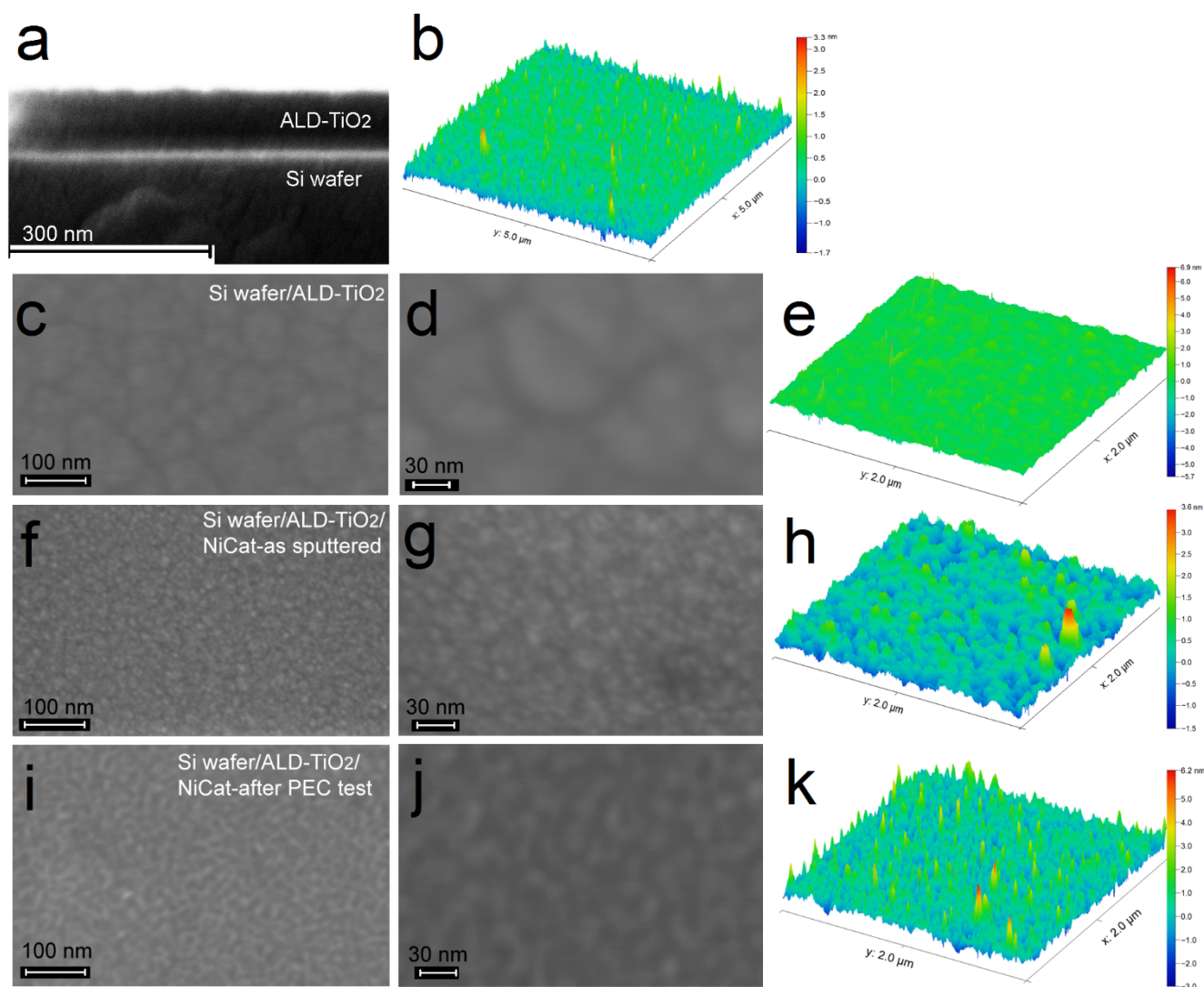


**Fig. S11** Morphology of the ALD-TiO<sub>2</sub> layer on Si wafer. (a) cross-sectional SEM image, (b) the 3D AFM topography image of the TiO<sub>2</sub> surface within a larger area (5.0 μm × 5.0 μm), (c) and (d) top-view SEM images, (e) the 3D AFM topography within a smaller area (2.0 μm × 2.0 μm). The ALD technique guarantees the excellent flatness of the TiO<sub>2</sub> layer, with thickness different no more than 1 nm. Morphology of the as-sputtered NiCat on TiO<sub>2</sub>: (f) and (g) top-view SEM images, (h) the 3D AFM topography image with an area of 2.0 μm × 2.0 μm. The NiCat layer is a non-continuous layer with an island morphology. The height of most NiCat islands is ~ 2 nm. Morphology of NiCat on TiO<sub>2</sub> after PEC measurements: (i) and (j) top-view SEM images, (k) the 3D AFM topography image with an area of 2.0 μm × 2.0 μm. The island morphology of NiCat remains after all PEC measurements, but in addition, the height becomes ~1 nm larger due to the oxidation of metallic Ni to Ni hydroxide and oxyhydroxide.<sup>9,10</sup>

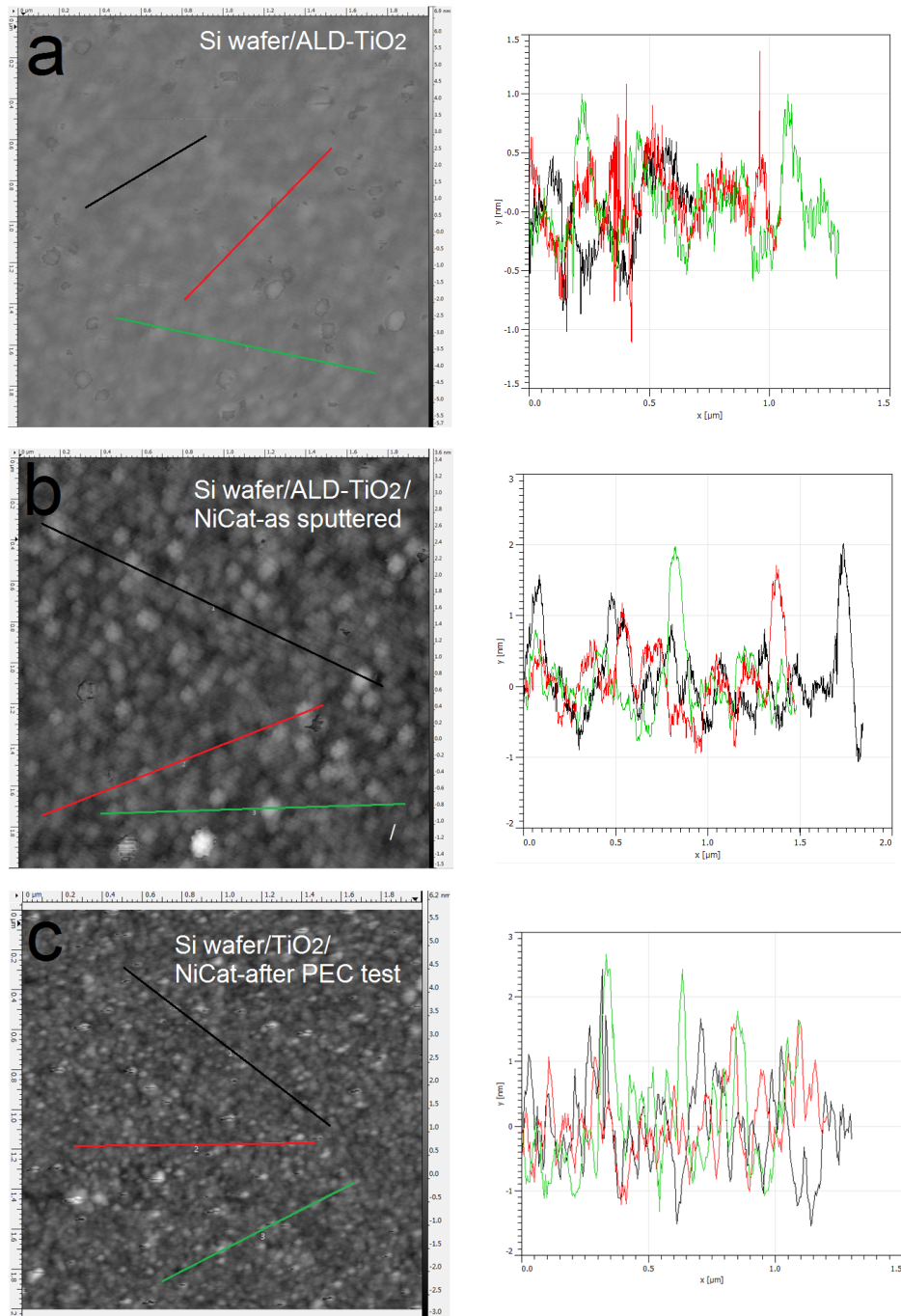


**Fig. S12** AFM topography images and height profiles of (a) the ALD-TiO<sub>2</sub> layer on Si wafer, (b) the as-sputtered NiCat on TiO<sub>2</sub> and (c) the NiCat on TiO<sub>2</sub> after PEC test. Again, the ALD-TiO<sub>2</sub> surface is very flat, and suggests that the layer is conformal. The as-sputtered NiCat has an island morphology, with a height of ~2 nm. After PEC test, the NiCat is expanded.

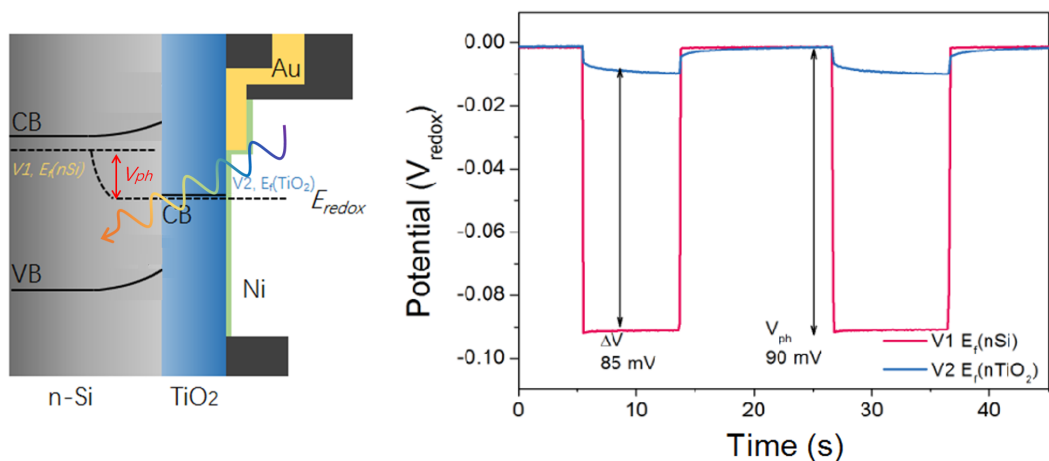


**Fig. S13** Determination of the  $V_{ph}$  generated by nSi/TiO<sub>2</sub> junction. Left: schematic of the band diagram of an nSi/TiO<sub>2</sub>/Ni DWE. V1 is the back contact potential, controlling  $E_f(\text{nSi})$ ; V2 is attached to the TiO<sub>2</sub>, controlling the  $E_f(\text{TiO}_2)$ . Right:  $V_{ph}$  determination in a  $[\text{Fe}(\text{CN})_6]^{4-}/[\text{Fe}(\text{CN})_6]^{3-}$  redox solution. Both V1 and V2 are kept at open circuit. In dark condition,  $E_f(\text{nSi})$  and  $E_f(\text{TiO}_2)$  are equilibrated with the solution redox potential. Hence V1 and V2 values are close to zero vs. redox in dark. Under illumination,  $V_{ph}$  is generated. The nSi quasi Fermi level for holes and  $E_f(\text{TiO}_2)$  are equilibrated with the solution redox, while nSi quasi Fermi level for electrons (V1) is up shifted. This is why V1 shows a large negative value and V2 doesn't change to much under illumination. The change of V1 is the  $V_{ph}$ , determined as 90 mV. The  $\Delta V$  is 85 mV. The tiny different can be due to the contact problems.

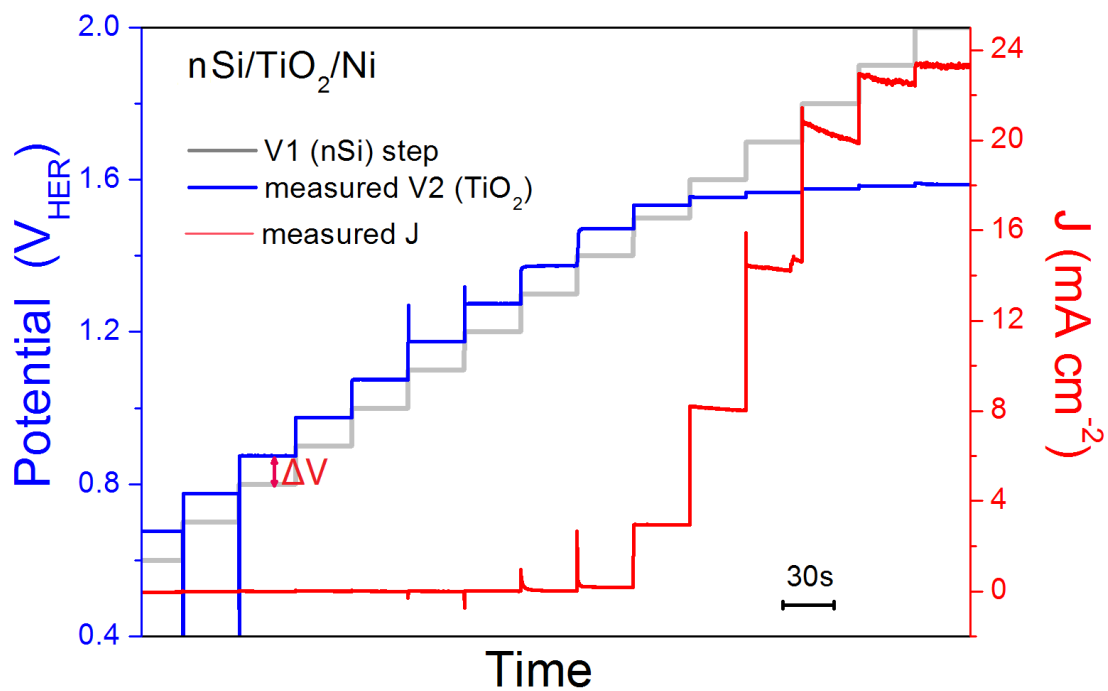


**Fig. S14**  $E_f(\text{TiO}_2)$  and J values and J values of nSi/TiO<sub>2</sub>/Ni photoanode with stepwise controlled V1.

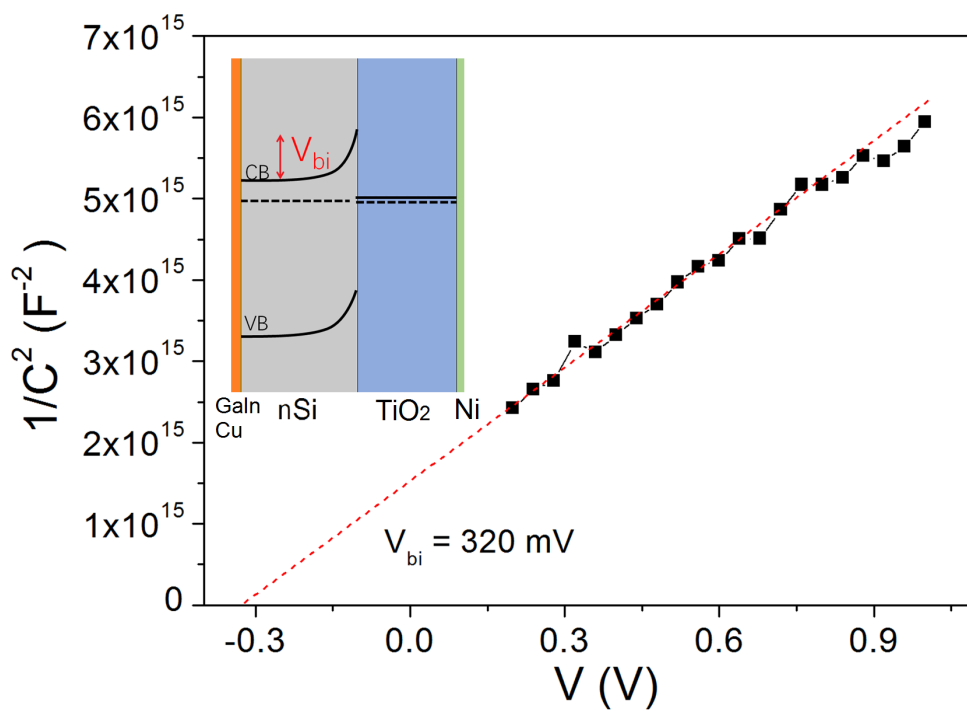


**Fig. S15** Mott-Schottky plot of the  $n\text{Si}/\text{TiO}_2$  electrode. The capacitance data are obtained from electrical impedance spectroscopy with two-electrode mode in dark condition. The inset is the structure of the electrode. Back contact is Galn eutectic and copper foil. Front contact is a 20 nm thick Ni metal layer. The  $V_{bi}$  of  $n\text{Si}/\text{TiO}_2$  junction is determined as 320 mV.

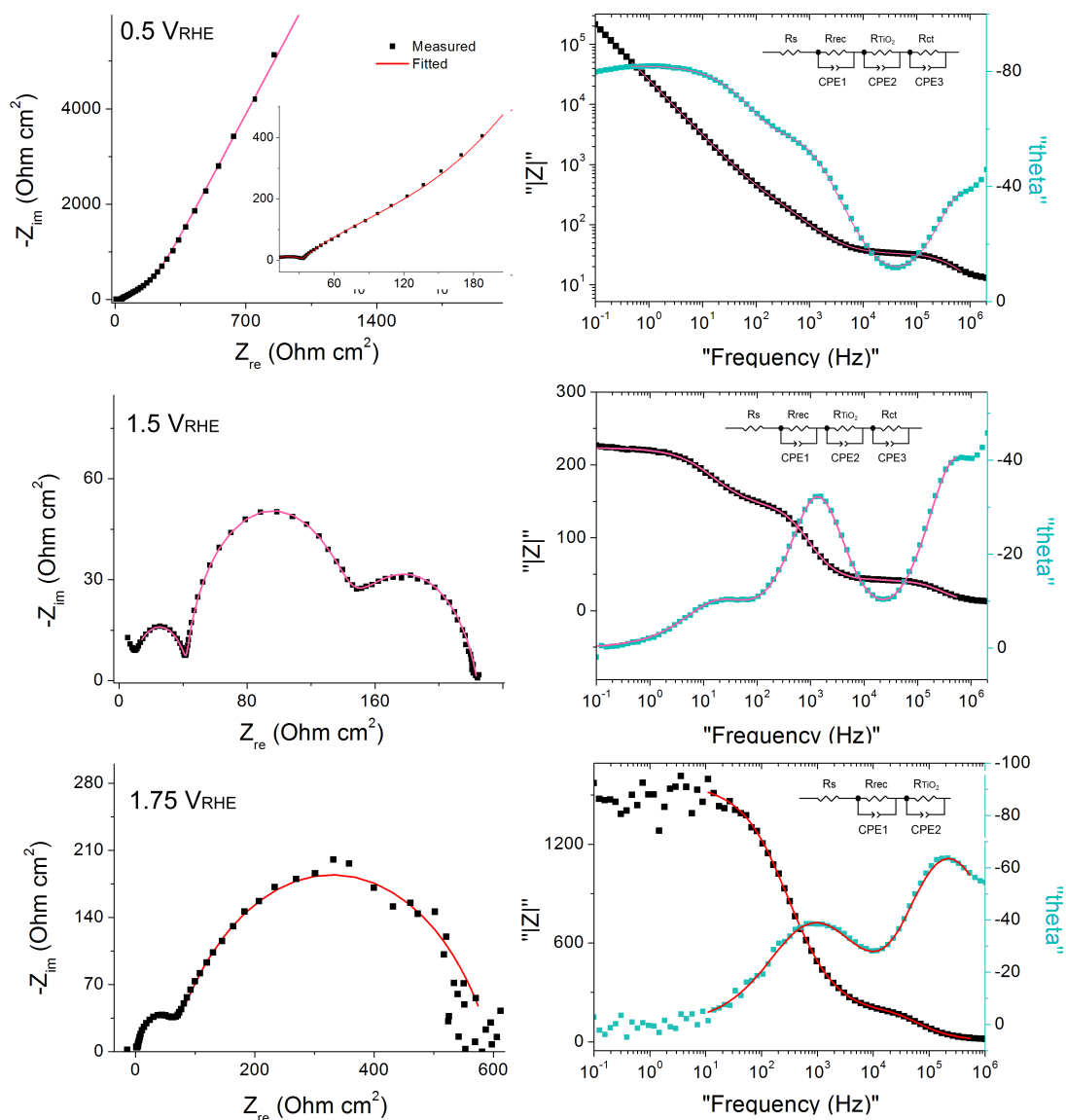


**Fig. S16** Nyquist and bode plots and corresponding fitting of an nSi/TiO<sub>2</sub>/Ni photoanode at back contact potentials of 0.55, 1.5 and 1.75 V<sub>RHE</sub> under one sun illumination. Equivalent circuit models are given as well.  $R_s$  is the series resistance raised by electrolyte solution.  $R_{rec}$  is the overall resistance of charge recombination taking place in the nSi.  $R_{TiO_2}$  is the overall resistance of charge transfer through the TiO<sub>2</sub> layer.  $R_{ct}$  is associated with the O<sub>2</sub>-evolving process at the Ni catalyst.

## REFERENCES

- 1 X. Li, J. Yu, J. Low, Y. Fang, J. Xiao and X. Chen, *J. Mater. Chem. A*, 2015, **3**, 2485–2534.
- 2 T. Moehl, J. Suh, L. Sévery, R. Wick-Joliat and S. D. Tilley, *ACS Appl. Mater. Interfaces*, 2017, **9**, 43614–43622.
- 3 A. Paracchino, N. Mathews, T. Hisatomi, M. Stefik, S. D. Tilley, M. Grätzel and M. Graetzel, *Energy Environ. Sci.*, 2012, **5**, 8673–8681.
- 4 A. V Naumkin, A. Kraust-Vass, S. W. Gaarenstroom and C. J. Powell, NIST X-ray Photoelectron Spectroscopy Database, National Institute of Standards and Technology.
- 5 S. Hu, M. R. Shaner, J. A. Beardslee, M. Lichterman, B. S. Brunschwig and N. S. Lewis, *Science (80-. )*, 2014, **344**, 1005–1009.
- 6 G. Mattioli, F. Filippone, P. Alippi and A. Amore Bonapasta, *Phys. Rev. B - Condens. Matter Mater. Phys.*, , DOI:10.1103/PhysRevB.78.241201.
- 7 S. H. Cheung, P. Nachimuthu, A. G. Joly, M. H. Engelhard, M. K. Bowman and S. A. Chambers, *Surf. Sci.*, 2007, **601**, 1754–1762.
- 8 W. Cui, W. Niu, R. Wick-Joliat, T. Moehl and S. D. Tilley, *Chem. Sci.*, 2018, **9**, 6062–6067.
- 9 C. Ding, J. Shi, Z. Wang and C. Li, *ACS Catal.*, 2017, **7**, 675–688.
- 10 M. R. Nellist, F. A. L. Laskowski, F. Lin, T. J. Mills and S. W. Boettcher, *Acc. Chem. Res.*, 2016, **49**, 733–740.